Vietnam Journal of Catalysis and Adsorption
Tạp chí xúc tác và hấp phụ Việt Nam

http://jca.edu.vn

Aluminum particles as anode material for lithium ion batteries: effect of particle sizes on the electrochemical behaviours

Kien Trung Pham[1], Tien Van Hoang[2], Thu Chau Uyen Le[4], Huyen Thi Nguyen[3], Thien Tri Vu[1], Thanh Huu Le[1], Dung Trung Dang[2], Hang Thi Thu Le[2], Tung Thanh Nguyen[3], Hung Tran Nguyen[1,*], Duong Duc La[1,*]

[1] *Institute of Chemistry and Materials, Nghia Do, Cau Giay, Hanoi, VIETNAM*
[2] *School of Chemistry and Life Sciences, Hanoi University of Science and Technology, 1 Dai Co Viet, Hanoi, VIETNAM*
[3] *Vietnam Academy of Science and Technology, 18 Hoang Quoc Viet, Hanoi, VIETNAM*
[4] *University of Science and Technology of Hanoi, 18 Hoang Quoc Viet, Hanoi, VIETNAM*
**Email: nguyentranhung28@gmail.com; duong.duc.la@gmail.com*

ARTICLE INFO

Received: 13/09/2024
Accepted: 24/09/2024
Published: 30/09/2024

Keywords:
Lithium-ion batteries; anode; aluminum, particles.

ABSTRACT

This study presents a preliminary investigation on using pristine aluminum particles as anodes for lithium-ion battery. The microstructural characteristics of aluminum particle samples with sizes from 100 nm (0.1 µm) to 70 µm were analyzed by the SEM and XRD methods. The electrochemical behaviors of the aluminum particles were examined by the cyclic voltammetry (CV) and galvanostatic charge/discharge (GCD) measurements. The obtained results demonstrated the distinct lithiation/delithiation features of the aluminum electrodes at the potential couple of around 0.25 V/0.50 V vs. Li/Li^+. Moreover, the GCD results also revealed the strong impact of the particle size on the initial capacity and galvanostatic discharge/charge potential profiles of electrode samples. However, aluminum electrodes with the large-sized particles showed dramatical capacity decay after certain cycles, and stabilized at around the specific capacity of 50 mAh g^{-1} and exhibited capacitive charge/discharge behavior. In contrast, the nano-sized particles aluminum electrodes possessed stable electrochemical performance upon cycling, but with low initial capacities. The results in this work will enrich the knowledge of the aluminum-based anode for LIBs in future works.

1. Introduction

After being commercialized for 30 years, the production of lithium-ion battery (LIB) has evolved into a significant industry, generating billions of dollars on a global scale. Initially, soft and hard carbon were used, but graphite has subsequently emerged as the preferred choice for the anode in today's commercial LIBs. Despite ongoing improvements to enhance performance and meet the demands of various applications for LIBs, the conventional graphite anode appears to reach its limitations. This is primarily due to inherent drawbacks, including a restricted theoretical capacity of 372 mAh g-1, the occurrence of exfoliation during lithiation resulting in capacity loss, and safety concerns arising from the formation of lithium metal dendrites [1]. The drawbacks have served as the impetus for new innovations, particularly when application requirements prioritize safety and capacity.

Scientists and engineers are continuously striving to enhance the performance of LIBs through various

https://doi.org/10.62239/jca.2024.061

approaches. One of the alternatives is experimenting with different materials to replace the commonly used graphite anode. Recently, alloying-type electrode materials have emerged as promising candidates for the next generation of anodes in LIBs due to significantly high theoretical capacities and less susceptibility to the formation of lithium dendrites. Aluminum (Al), the second most plentiful element found in the earth's crust, is widely manufactured on a global scale for various applications. Since the 1970s, it has been reported that aluminum exhibits characteristics of an alloying-type anode [2–4]. According to the previously published literatures indicates that aluminum combines with lithium (Li) to create Li-rich intermetallic compounds viz., LiAl, Li_3Al_2, Li_9Al_4 at low equilibrium potentials (0.23–0.38 V vs. Li/Li^+), resulting in theoretical specific capacities of 993, 1490, and 2234 mAh g^{-1}, respectively. These values are significantly higher than that of a graphite anode [5]. In addition, Al-based anodes can address the safety issue of lithium dendrites by forming an alloy with Li at a higher potential than the intercalation potential of graphite.

To realize the application potential of aluminum material as anode for LIBs, numerous unique designs of anodes have been performed [6,7]. Despite the superior performance, these approaches remain excessively complex and expensive to implement on a larger scale. To commercialize aluminum-based anodes for LIBs, it is crucial to streamline the manufacturing process, from material selection to fabrication of end products. The electrode active material is commonly in the form of small particles. However, the process of selecting an appropriate particle size can be a complex decision that requires careful optimization. The electrode active materials with large particles are easy to prepare, but they result in unstable electrode structures and are more prone to fracturing due to volume expansion during cycling. Conversely, for the electrode active materials with smaller particles the electrode pulverization phenomenon can be restricted. The electrochemically active area of the electrodes can be enhanced owing to the high surface area of the electrode active material, but the complexity of the preparation process increase as well [8,9].

To date, several works reported on the electrochemical performance of pure aluminum material as anode for LIBs [6]. To our best knowledge, reports on evaluation of the effect of the aluminum particles size on their electrochemical performance behavior in LIBs are insufficient. To expand the knowledge on the electrochemical behaviors (i.e. working mechanism, cycling stability, charge/discharge capacity) of alloying-type anode materials like aluminum metal as well as to approach industrial scale, investigation on using directly the commercial products of aluminum particles as anode materials for LIBs is essential. This work reports on the effect of the particle size of the commercial aluminum powder products on the electrochemical performance for anode materials in LIBs.

2. Experimental

Chemical and materials

Aluminum powder samples with 99.9 % purity and different sized particles ranging from 100 nm (0.1 µm), 2 µm, 5 µm, 10 µm, 20 µm to 70 µm were used in this study. These powder samples were labelled as Al-0.1 µm, Al-2 µm, Al-5 µm , Al-10 µm, Al-20 µm and Al-70 µm, respectively. Besides, other chemicals and materials including Polyvinylidene fluoride (PVDF), N-Methyl-2-pyrrolidone (NMP), black carbon Super P used in this study were acquired from TMax company (China).

Physicochemical characterizations

Scanning electron microscopy (SEM) were used to survey the surface morphology of aluminum particles. The SEM images were acquired by HITACHI S-4800 system. Crystallinity structure and elemental purity of the samples were confirmed by X-Ray diffraction (XRD) in the Bruker D8 Advance system.

Electrochemical characterizations

Powdery aluminum samples were used directly to fabricate working electrodes without any further modification. A mixture of 70 %w aluminum powder, 20 %w black carbon Super P, and 10 %w PVDF were mixed well with an adequate amount of NMP solvent in a ball mill for 1 h to form a homogeneous slurry. The slurry was then blade cast onto a carbon coated copper foil. After being dried at 80 ^oC for 8 h, the foil was cut into dishes of 10 mm in diameter, which were utilized as working electrodes in electrochemical tests. CR2032 coin half cells were assembled in an argon-filled glovebox. A Li metal foil was used as counter and reference electrode, and a circle piece of Polypropylene (TMax, China) was used as separator, which was soaked with 1M $LiPF_6$ in a solvent mixture of ethylene carbonate (EC), dimethyl carbonate (DMC), diethyl carbonate (DEC) (battery grade, TMax, China). The volume ratio of EC:DMC:DEC was 1v:1v:1v.

The lithiation/delithiation behavior of the aluminum electrodes was recorded by using cyclic voltammetry (CV) at a scan rate of 0.05 mV s^{-1}. Cycling performance

https://doi.org/10.62239/jca.2024.061

of the electrodes were examined by the galvanostatic charge-discharge (GCD) technique at a specific current of 50 mA g^{-1}. CV and GCD measurements were conducted on the WonATech-WBCS 3000L32 system.

3. Results and discussion

Physicochemical characterizations

First, confirming some characteristics such as morphology, crystallinity and purity of the aluminum powder are needed. Fig 1 shows the XRD patterns of the commercial aluminum powder samples. It is obvious that, the XRD patterns of all the aluminum samples possess three strong diffraction peaks at the 2θ values of 38.45°, 44.71°, and 65.09°, which is corresponding to the (111), (200) and (220) planes, respectively. These peaks are totally coincided with the standard lines of metallic aluminum (JCPD No. 01-089-2769). This confirms the cubic crystal structure of the aluminum power samples. The XRD results obtained in the present work is in high agreement with the previous report [10].

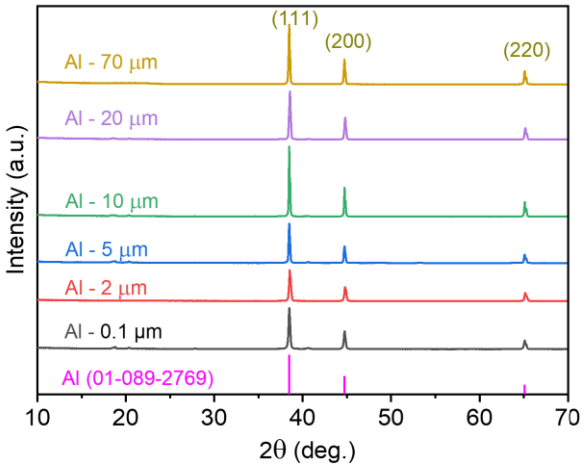

Fig 1: XRD patterns of different aluminum samples

Fig 2 presents the SEM images of the aluminum powder samples at different magnifications. Obviously, the spherical-shaped particles are observed for all the commercial aluminum powder samples. In general, the aluminum particles are relatively uniform. Apart from the Al-0.1 µm and Al-2 µm samples, the surface of the remaining samples appears rough. This may be due to differences in the manufacturing parameters as well as manufacturing technology of the different suppliers. It is noteworthy that, because of the high activity of metallic aluminum, there is always existence of a thin layer of aluminum oxide, namely alumina, forming naturally once metallic aluminum is exposed to the ambient air. Normally, the thickness of the alumina layer is about 4-5 nm [11]. Therefore, under restricted storage, the presence of a certain amount of alumina in the metallic aluminum powder is inevitable.

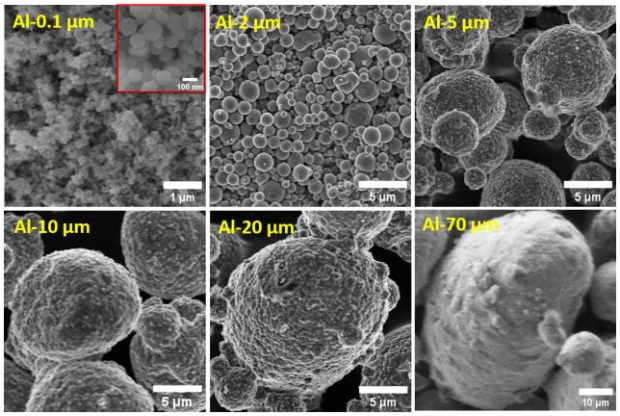

Fig 2: SEM images of the aluminum powder samples.

3.2. Electrochemical behaviors

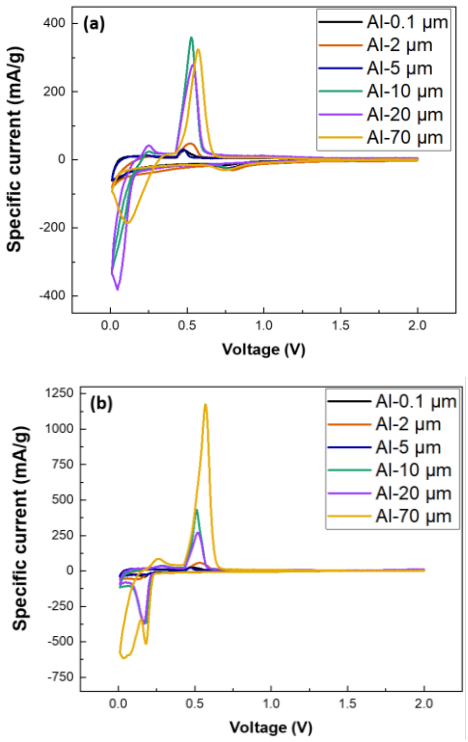

Fig 3: CV curves of the aluminum electrodes: (a) Al-0.1 µm, (b) Al-2 µm, (c) Al-5 µm, (d) Al-10 µm, (e) Al-20 µm, (f) Al-70 µm; and (g) the first and (h) second cycle of all samples in comparison.

To investigate the lithiation/delithiation mechanism of the commercial powdery aluminum as anode material for LIBs, the aluminum electrodes fabricated from the aluminum powder with different sizes were examined by the CV method at the scan rate of 0.05 mV s^{-1} from 0.01 V to 2.0 V *vs.* Li/Li^+. Fig 3 displays the cyclic voltammograms of the electrodes. In the cathodic

scan, at the first cycle, a reduction peak was recorded at around the potential of 0.78 V, indicating the irreversible formation of solid electrolyte interphase (SEI) [5]. The cathodic peak at 0.78 V was only found for the electrodes of the aluminum powder samples with the small particle size in a range of 0.1 µm -10 µm. This can be explained by the high surface area of the aluminum powder with the small particle size facilitated more SEI formation reaction to occur, resulting in higher peak current recorded in the voltammograms. Meanwhile, for the aluminum electrodes of the large particle sizes such as Al-20 µm and Al-70 µm with lower surface area, the irreversible reduction peak was hardly observed. From the second cycle onwards, the this peak disappeared, implying that the SEI formation was almost only formed at the initial cycle.

However, at the low potential region, the electrodes show another sharp reduction peak at the potential lower than 0.25 V, which represents the alloying process of Al and Li to form β-LiAl at room temperature (i.e. $Li^+ + e^- + Al = LiAl$) [5]. Interestingly, this reduction peak seems to have tendency to shift toward the direction of more negative potential (see Fig 3a). Even, a loop appears on the CV curve of the Al-70 µm electrode. This can be attributed to the existence of the alumina layer covering the metallic aluminum particles. According to the previous report [6], upon the first lithiation, the aluminum oxide absorbed Li to irreversibly form a Li-Al-O glass layer, which has the ability to transfer Li^+ ion into the material bulk with the diffusion coefficient of the order of 10-14 $cm^2\ s^{-1}$ [12]. The lithiation overpotential of Al_2O_3 is significant, leading to the shift of the cathodic peak and appearance of the CV loop in the first cycle. This peak phenomenon fades in the subsequent cycles (see Fig 3b), indicating that the lithiation of Al_2O_3 is complete and establishing a channel for Li^+ to migrate inside the active material particles. Remarkably, as seen in Fig 3b, the voltammogram for the second cycle of the Al-70 µm electrode exhibits another prominent reduction peak at near 0.01 V, suggesting that the initial alloying process of pristine aluminum material to form β-LiAl still occurred. This results from the extremely large particle size of the aluminum powder.

In the anodic scan, a sharp oxidation peak was at around 0.5 V. This peak is characteristic for the de-alloying of β-LiAl phase [13].

Fig 4 illustrates the charge/discharge performance of the aluminum electrodes at a specific current of 50 mA g^{-1} for 100 cycles. At the first glance, the electrodes reveal the same behavior. At several first cycles, the electrodes possessed the highest specific capacity, corresponding to the lowest coulombic efficiency as a significant amount of Li was consumed to form SEI and the Li-Al-O glass layer. In specific, the highest specific charge capacity of 490 mAh g^{-1}, 320 mAh g^{-1}, 280 mAh g^{-1} was measured for the Al-70 µm, Al-20 µm and Al-10 µm electrodes, respectively.

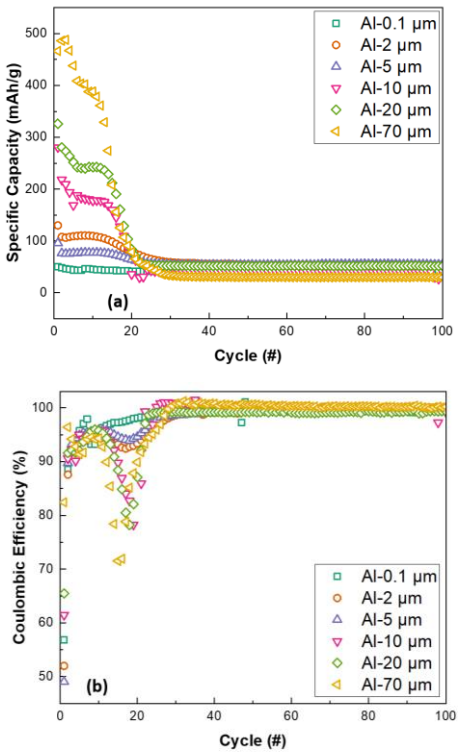

Fig 4: Galvanostatic charge/discharge performance of the aluminum electrodes at the specific current density of 50 mA g^{-1}: (a) cyclability and (b) coulombic efficiency

Meanwhile, for the electrodes with the small particle size such as the Al-5 µm, Al-2 µm and Al-0.1 µm, the specific charge capacity that the electrodes delivered at the first cycle was 100 mAh g^{-1}, 130 mAh g^{-1}, 50 mAh g^{-1}, respectively. During the next 20 – 30 cycles, the electrodes witnessed a significant decline in capacity. Then specific capacity stabilized at approximately 50 mAh g^{-1}. Hence, it is obvious that the electrodes with the large particle size offered the high specific capacity compared with those having the small particle size. This is related to the lower coulombic efficiency of the electrodes with the small particle size (Fig 4b), which results from the high surface area of the aluminum powder. Nevertheless, the obtained specific capacity of all samples appeared to be much lower than the theoretical capacity of aluminum material (~993 mAh g^{-1}). This can be explained as the mass of inevitable innert Al_2O_3 layer in the electrode material reduces the specific capacity in the calculation. This implication also

https://doi.org/10.62239/jca.2024.061

suggest that by eliminating the Al_2O_3 layer prior to the electrode fabrication process is necessary to improve calculated specific capacity. Regardless of deviation in the particle size of the electrodes, their capacity almost stabilized at the same level after cycling.

Interestingly, the specific capacity of the electrode of the micron-sized aluminum powder samples was recorded to have another significant drop just after 10 cycles of stabilization (Fig 4a), accompanied by a respective decline in coulombic efficiency (Fig 4b). While the formation of the SEI and Li-Al-O glass layers were accountable for the first decrease, the second reduction was caused by another mechanism. It is widely accepted that alloying-type anode materials (Al, Si, Sn, Ge…) face detrimental effect from volume expansion and contraction during the cycling process [14]. The bigger the particle size was, the more likely the internal stress derived from volume shift of alloy phase was thought to cause fractures in the material bulk, ultimately leading to cell fading due to loss of electrical connection. Therefore, the forementioned decline starting at around the 17th cycle was caused by anode material fragmentation and loss of electrical connection. Additionally, following pulverization of the aluminum particles, the crystalline lattice of fresh aluminum was exposed to electrolyte and formed a new SEI layer, resulted in irreversible capacity loss and lowered coulombic efficiency. In contrast, nanostructured anode materials was resilient to negative effect of the accumulation of internal strain stress caused by volume change during cycling [15]. Undeniably, the Al-0.1 µm sample supplied the relatively low initial capacity compared to others, but its capacity hardly degraded. Therefore, there must be another reason behind the capacity fading rather than the pulverization and electrical disconnection.

To explore this phenomenon further, the GCD potential profile of the electrodes was examined. As shown in Fig 6a, at the first cycle, the discharge potential profile of the electrodes with the large sized particles such as Al-10 µm, Al-20 µm and Al-70 µm shows a significantly wide plateau leveling at around 0.2 V and a minor plateau at around 0.78 V, corresponding to the initial lithiation and SEI formation processes. The discharge potential curve of the Al-0.1 µm electrode, in contrast, only presents a short plateau, implying the formation of the SEI layer. The rest of the discharge curve is steep and similar to the discharge curve of capacitors. Herein, the short plateau at around 0.78 V of the electrodes totally disappears in the second discharge, indicating that the SEI layer was completely established during the first discharge. Noticeably, immediately preceding to the wide plateau, a small dip in the potential is observed for the first discharge. This phenomenon has been also reported in the previous report [6]. Accordingly, this potential dip is believed to stem from the nucleation energy barrier. According to the obtained empirical data in this study, it is claimed that the potential dip is proportional to the particle size of the aluminum material. Wherein, the Al-70 µm sample exhibits the considerable potential drop of 119 mV while the drop is negligible for the remaining samples, for example, 0.4 mV for the Al-5 µm, 67 mV for the Al-10 µm, and 86 mV for the Al-20 µm (Fig 5c). The discharge potential dip is still observable in the second cycle but at an inferior extent, indicating the continuing nucleation and growth of the alloy phase [16]. For the Al-0.1 µm sample, no potential dip is detected in the first cycle, indicating that the overpotential of the nucleation is not significant for the nano-scale particles. Accordingly to Hudak and Huber, the small sized materials characterized surface reactions, thus supplied insignificant practical capacity compared to the theoretical capacity [17]. In contrast, the large sized materials showed the bulk alloying reaction and could offer the practical capacity comparable to the theoretical capacity. From the 50th cycle onwards (Fig 5a), the discharge plateaus absolutely disappear, replaced by the sloop curves which are characteristic for capacitors.

For the charge stage, the similar trend was recognized for the electrodes of the micron sized aluminum samples. The samples present a distinct charge plateau at around 0.5 V, corresponding to the dealloying of LiAl (Fig 5b) while the Al-0.1 µm electrode only possesses capacitive feature. After 50 cycles, the alloying and dealloying were degraded. The sharp plateau in the charge potential profiles of the micron sized samples are no longer observable and almost identical with that of the Al-0.1 µm (Fig 5b). Therefore, it can be concluded that, after some cycles of discharge and charge, the morphology of the micron-sized samples changed and quickly reached the comparable particle size. The achieved results in the present work is also consistent with the literature [18]. Regarding this "pseudo-capacitive" properties, according to Kwon and coworkers, after many cycles the aluminum electrode would be pulverized and converted to nano scale grain structures [19]. Nevertheless, some perspectives suggested that the phenomenon was attributed to the amorphization of aluminum and converted to a porous phase after many repetitive cycles of discharge-charge [15,18]. Porous amorphous anode materials are hardly equivalent to the crystalline phase in alloying capacity but can be very resilient to repeated cycles. Based on the resultant figures in the present work,

https://doi.org/10.62239/jca.2024.061

it is evidenced that choosing a suitable particle size is critical to achieve an optimum balance between capacity and stability parameters, especially for the commercialization purposes.

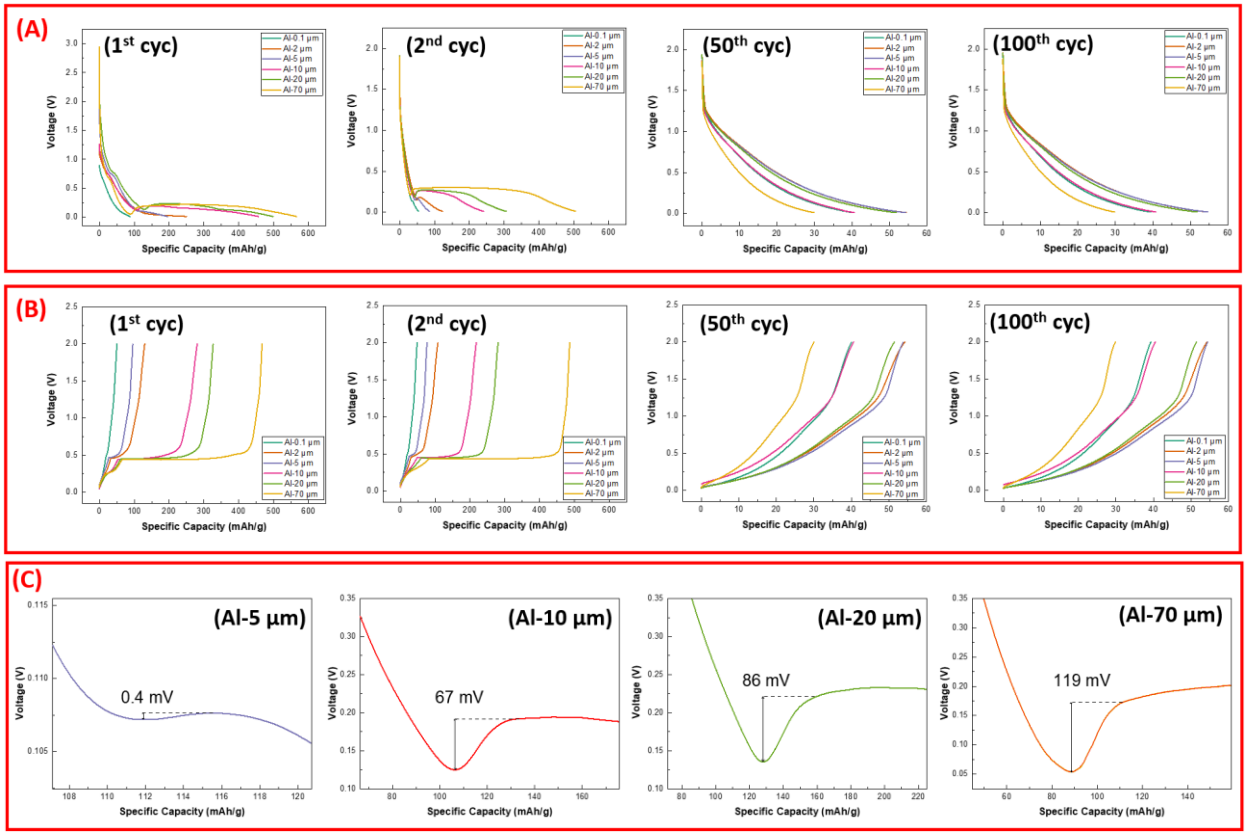

Fig 5: (A) discharge, (B) charge potential profiles of the aluminum electrodes at different cycles; and (C) illustration of the potential dip of the aluminum electrodes at the first discharge.

4. Conclusion

In the present work, the feasibility of using aluminum powder with different particle sizes as anode material for LIBs has been examined. The attained results demonstrated that, all aluminum powder samples possessed the alloying/dealloying capability with lithium. The powder samples with the large particles offered significant capacity with more distinct discharge-charge plateaus. Yet, the specific capacity of the micron sized samples degraded after about 20-30 cycles and stabilized at around 50 mAh g^{-1}, along with capacitive-like charge and discharge potential profiles. The capacity decay rate was magnified as the size of the aluminum particles increased. The observed phenomenon suggested that, (i) the size of the aluminum particles determined the initial capacity of the electrodes and the lithiation/delithiation nature; and (ii) for long term cyclability, the electrochemical behavior of the aluminum samples with the large size particles was comparable to the sample with the nano sized particles because of the pulverization and/or amorphourization during cycling. Ultimately, the pristine metallic aluminum powder needs modifying further to become a viable anode material for LIBs.

Acknowledgements

This research is funded by Vietnamese Government under project numbered 001.2023.ĐT.CNKK.QG.

References

1. Hang L. T. T., Huyen N. T. T., Thuy H. T. B., Vietnam Journal of Catalyst and Adsorption 9 (2020) 114–119.
2. B. M. L. Rao, R. W. Francis, H. A. Christopher, J. Electrochem. Soc. 124 (1977) 1490–1492. https://doi.org/10.1149/1.2133098
3. E. C. Gay, D. R. Vissers, F. J. Martino, K. E. Anderson, J. Electrochem. Soc. 123 (1976) 1591–1596. https://doi.org/10.1149/1.2132652
4. C. A. Melendres, C. C. Sy, J. Electrochem. Soc. 125 (1978) 727–731. https://doi.org/10.1149/1.2131536
5. T. Zheng, J. Zhang, X. Guo, W. Jin, S. T. Boles, Electrochimica Acta 485 (2024) 144127. https://doi.org/10.1016/j.electacta.2024.144127

6. H. Wang, H. Tan, X. Luo, H. Wang, T. Ma, M. Lv, X. Song, S. Jin, X. Chang, X. Li, J. Mater. Chem. A 8 (2020) 25649–25662. https://doi.org/10.1039/D0TA09762D
7. B. Sun, Y. Xu, S. Yang, D. Zhang, C. Pei, S. Ni, Mater. Chem. Front. 7 (2023) 2554–2569. https://doi.org/10.1039/D2QM01283A
8. M. Yoshio, T. Tsumura, N. Dimov, Journal of Power Sources 163 (2006) 215–218. https://doi.org/10.1016/j.jpowsour.2005.12.078
9. X. H. Liu, L. Zhong, S. Huang, S. X. Mao, T. Zhu, J. Y. Huang, ACS Nano 6 (2012) 1522–1531. https://doi.org/10.1021/nn204476h
10. X. Lei, J. Ma, J. Braz. Chem. Soc. 21 (2010) 209–213. https://doi.org/10.1590/S0103-50532010000200004
11. X. Chang, Z. Xie, Z. Liu, X. Zheng, J. Zheng, X. Li, Nano Energy 41 (2017) 731–737. https://doi.org/10.1016/j.nanoen.2017.10.017
12. G. Oltean, C.-W. Tai, K. Edström, L. Nyholm, Journal of Power Sources 269 (2014) 266–273. https://doi.org/10.1016/j.jpowsour.2014.06.118
13. M. Z. Ghavidel, M. R. Kupsta, J. Le, E. Feygin, A. Espitia, M. D. Fleischauer, J. Electrochem. Soc. 166 (2019) A4034–A4040. https://doi.org/10.1149/2.0061916jes
14. M. N. Obrovac, V. L. Chevrier, Chem. Rev. 114 (2014) 11444–11502. https://doi.org/10.1021/cr500207g
15. M. Nieradko, L. Eskandarian, O. A. Semenikhin, Electrochimica Acta 327 (2019) 135023. https://doi.org/10.1016/j.electacta.2019.135023
16. T. Zheng, D. Kramer, M. H. Tahmasebi, R. Mönig, S. T. Boles, ChemSusChem 13 (2020) 974–985. https://doi.org/10.1002/cssc.201903060
17. N. Hudak, D. Huber, ECS Trans. 33 (2011) 1–13. https://doi.org/10.1149/1.3557706
18. X. Chang, Z. Xie, Z. Liu, X. Zheng, J. Zheng, X. Li, Energy Storage Materials 25 (2020) 93–99. https://doi.org/10.1016/j.ensm.2019.10.027
19. G. D. Kwon, E. Moyen, Y. J. Lee, J. Joe, D. Pribat, ACS Appl. Mater. Interfaces 10 (2018) 29486–29495. https://doi.org/10.1021/acsami.8b08358